ELSEVIER

Catalysis Today 66 (2001) 233–240

CATALYSIS TODAY

www.elsevier.com/locate/cattod

Hydrodynamics of reactive distillation tray column with catalyst containing envelopes: experiments vs. CFD simulations

J.M. van Baten, J. Ellenberger, R. Krishna*

Department of Chemical Engineering, University of Amsterdam, Nieuwe Achtergracht 166, 1018 WV Amsterdam, The Netherlands

Abstract

We have studied the hydrodynamics of a reactive distillation sieve tray column in which catalyst containing wire-gauze envelopes are disposed along the liquid flow direction. The gas and liquid phases are in cross-current contact on the tray. Experiments were carried out to determine the clear liquid height on the tray as a function of tray geometry and operating conditions. The transient gas–liquid hydrodynamics on the tray was simulated using CFD techniques. The agreement between the experiments and CFD simulations was found to be very good, suggesting that CFD simulations can be used for design and scale-up purposes.

Keywords: Structured packing; Residence time distribution; Computational fluid dynamics; Sieve trays; Clear liquid height; Froth height; Froth density

1. Introduction

There is a great deal of industrial interest in reactive distillation [1]. For heterogeneously catalysed liquid phase reactions, the liquid phase has to be brought into intimate contact with catalyst particles. Both packed columns (random packed or structured) and tray columns could be used [1–6]. In order to avoid diffusional limitations, the catalyst particles have to be smaller than about 3 mm in size. Such catalyst particles are usually encased within wire-gauze envelopes as in the KATAPAK-S and KATAMAX constructions of Sulzer Chemtech and Koch-Glitsch [2–4,7–12]. An alternative to the KATAPAK-S and KATAMAX construction is to dispose the wire gauze containing catalyst parcels along the liquid flow direction of a sieve tray distillation column as shown in Fig. 1(a) and (b). The liquid hold-up is usually much higher in sieve tray columns as compared to packed columns and this is an advantage when carrying out relatively slow, catalysed, liquid phase reactions. A further advantage of a catalytic sieve tray construction is that the contacting on any tray is *cross-current* and for large diameter columns, there will be a high degree of staging in the liquid phase; this is advantageous from the point of view of selectivity and conversion. Of course, from an overall point of view, in a multi-stage catalytic sieve tray column the vapour–liquid contacting is *counter-current*. The catalytic sieve tray construction has been patented [13] and is being used in industrial practice, there is no published information on the hydrodynamics of such contacting devices. The present study was undertaken to fill this much-needed gap. We use both experiments and CFD simulations to study the gas–liquid hydrodynamics.

* Corresponding author. Tel.: +31-20-525-7007; fax: +31-20-525-5604.
E-mail address: krishna@its.chem.uva.nl (R. Krishna).

0920-5861/01/$ – see front matter
PII: S0920-5861(00)00625-8

Nomenclature

C_D	drag coefficient (–)
d_G	diameter of gas bubble (m)
g	acceleration due to gravity (9.81 m/s^2)
h_{cl}	clear liquid height (m)
h_w	weir height (m)
M	inter-phase momentum exchange term (N/m^3)
p	pressure (N/m^2)
Q_L	liquid flow rate across tray (m^3/s)
u	velocity vector (m/s)
U_G	superficial gas velocity (m/s)
V_{slip}	slip velocity between gas and liquid (m/s)
W	weir length (m)

Greek letters

ε	volume fraction of phase (–)
μ	viscosity of phase (Pa s)
ρ	density of phases (kg/m^3)
τ	stress tensor (N/m^2)

Subscripts

cl	clear liquid
G	referring to gas phase
k	index referring to one of the three phases
L	referring to liquid phase
slip	slip

Superscript

B	from Bennett correlation

2. Experimental

The experimental set-up is shown in Fig. 1(c), which consists of a rectangular sieve tray and ancillary gas and liquid distribution devices. On the sieve tray, four containers (containing 1.1 mm glass spheres) are mounted. The sieve tray consists of 132 holes of 5 mm diameter. Experiments were also carried out without the four catalyst containers; in this case, the number of holes on the trays is 276. A calibrated rotameter (8) is used to control the gas flow rate (7). The gas enters the sieve tray trough a 0.025 m diameter copper tube, which has a chimney on top to ensure uniform outflow of gas. The liquid from the storage tank (2) is fed to the downcomer (6) by means of a centrifugal pump (3). The liquid flow rate is measured by a calibrated liquid flowmeter (4). Weir heights, h_w, of 60, 80 and 100 mm were used in the experiments. The liquid inlet tube (5) with an inner diameter of 15 mm is placed above the downcomer (6) and distributes the liquid uniformly over the downcomer. For a specified set of operating conditions, the dispersion height is read from the graduated scale attached to the side of the tray. To measure clear liquid height, h_{cl}, the gas inlet and liquid inlet are simultaneously, and instantly, switched off. The clear liquid height is read from the graduated scale attached to the side of the tray after a short period to allow for releasing the gas bubbles from the liquid. Demineralized water was used in the experiments. Further details of the experimental set-up, including photographs of the rig, and measurement technique are available on our web site: http://ct-cr4.chem.uva.nl/kattray.

3. CFD simulations

In order to describe the hydrodynamics, we also undertook CFD simulations. The model development is essentially the same as described in earlier work [5,6]. For either gas or liquid phases in the two-phase dispersion on the tray, the volume-averaged mass and momentum conservation equations are given by

$$\frac{\partial(\varepsilon_k\rho_k)}{\partial t} + \nabla\cdot(\rho_k\varepsilon_k\mathbf{u}_k) = 0,$$

$$\frac{\partial(\rho_k\varepsilon_k\mathbf{u}_k)}{\partial t} + \nabla\cdot(\rho_k\varepsilon_k\mathbf{u}_k\mathbf{u}_k - \mu_k\varepsilon_k(\nabla\mathbf{u}_k+(\nabla\mathbf{u}_k)^{\mathrm{T}})) = -\varepsilon_k\nabla p + \mathbf{M}_{k,j} + \rho_k\varepsilon_k\mathbf{g}$$

where ρ_k, $\mathbf{u}_k$, ε_k and μ_k represent, respectively, the macroscopic density, velocity, volume fraction and viscosity of the kth phase (=G or L), p the pressure, $\mathbf{M}_{k,j}$, the inter-phase momentum exchange between j and k phases, and $\mathbf{g}$ the gravitational force. The gas and liquid phases share the same pressure field, $p_G = p_L$. For the continuous, liquid, phase, the turbulent contribution to the stress tensor is evaluated by means of k–ε model, using standard single phase parameters $C_\mu = 0.09$, $C_{1\varepsilon} = 1.44$, $C_{2\varepsilon} = 1.92$, $\sigma_k = 1$ and

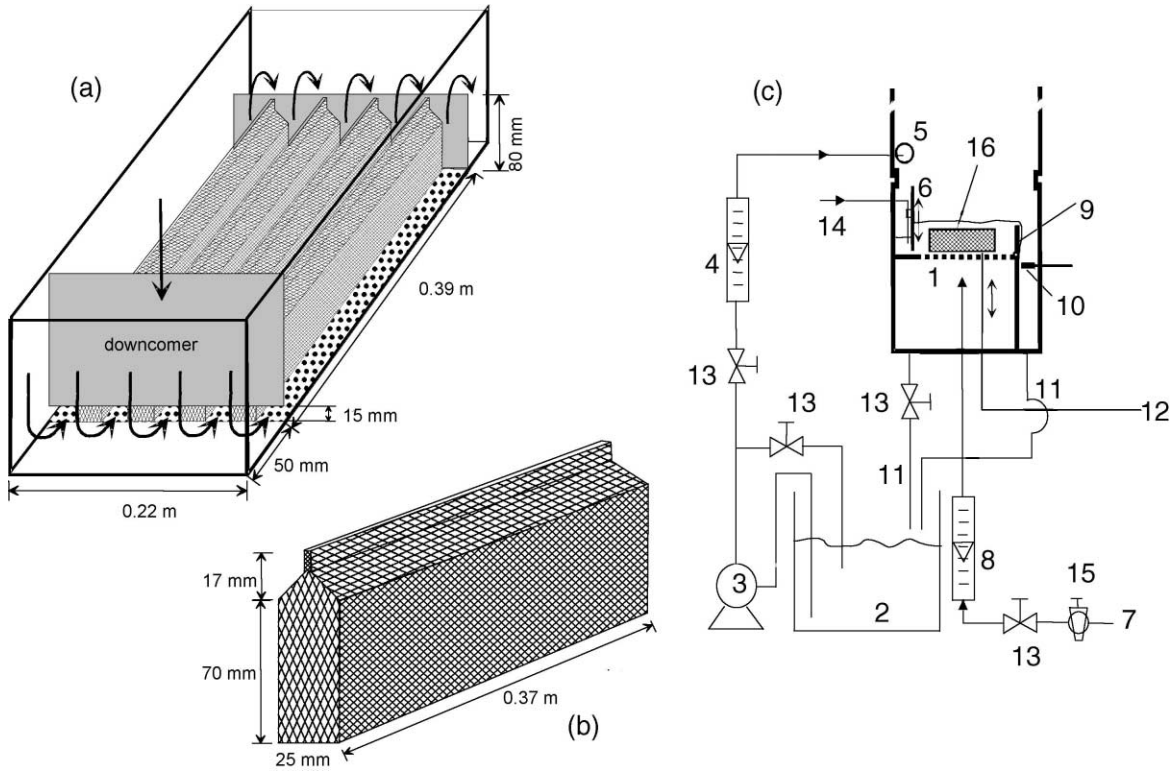

Fig. 1. (a) Sieve tray with catalyst filled containers in a wire-gauze envelope. (b) Details of container. (c) Experimental set-up for measurements of clear liquid height.

$\sigma_\varepsilon = 1.3$. No turbulence model is used for calculating the velocity fields within the dispersed gas phase. For gas–liquid bubbly flows the inter-phase momentum exchange term is

$$\mathbf{M}_{\mathrm{L,G}} = \frac{3}{4}\rho_{\mathrm{L}}\frac{\varepsilon_{\mathrm{G}}}{d_{\mathrm{G}}}C_{\mathrm{D}}(\mathbf{u}_{\mathrm{G}} - \mathbf{u}_{\mathrm{L}})|\mathbf{u}_{\mathrm{G}} - \mathbf{u}_{\mathrm{L}}|$$

where C_{D} is the inter-phase momentum exchange coefficient or drag coefficient. For the air–water system, the bubble rise velocity depends on the size and morphology of the bubbles [14–17]. For the high gas velocities normally used for operation on trays, the hydrodynamics corresponds to that of a bubble column operating in the churn-turbulent regime [18–22]. Following our earlier work, we estimated the drag coefficient of a swarm of bubbles using

$$C_{\mathrm{D}} = \frac{4}{3}\frac{\rho_{\mathrm{L}} - \rho_{\mathrm{G}}}{\rho_{\mathrm{L}}}gd_{\mathrm{G}}\frac{1}{V_{\mathrm{slip}}^2}$$

where V_{slip} is the slip velocity of the bubble swarm with respect to the liquid, $V_{\mathrm{slip}} = |\mathbf{u}_{\mathrm{G}} - \mathbf{u}_{\mathrm{L}}|$. The slip between gas and liquid can be estimated from superficial gas velocity and the gas hold-up $V_{\mathrm{slip}} = U_{\mathrm{G}}/\varepsilon_{\mathrm{G}}$. In this work, we use the Bennett et al. [23] correlation to estimate the liquid hold-up:

$$\varepsilon_{\mathrm{L}}^{\mathrm{B}} = \exp\left[-12.55\left(U_{\mathrm{G}}\sqrt{\frac{\rho_{\mathrm{gas}}}{\rho_{\mathrm{liq}} - \rho_{\mathrm{gas}}}}\right)^{0.91}\right]$$

with $\varepsilon_{\mathrm{G}}^{\mathrm{B}} = 1 - \varepsilon_{\mathrm{L}}^{\mathrm{B}}$.

In our CFD code, we used

$$\mathbf{M}_{\mathrm{L,G}} = \varepsilon_{\mathrm{G}}\varepsilon_{\mathrm{L}}(\rho_{\mathrm{L}} - \rho_{\mathrm{G}})g \times \frac{1}{(U_{\mathrm{G}}/\varepsilon_{\mathrm{G}}^{\mathrm{B}})^2}\frac{1}{\varepsilon_{\mathrm{L}}^{\mathrm{B}}}(\mathbf{u}_{\mathrm{G}} - \mathbf{u}_{\mathrm{L}})|\mathbf{u}_{\mathrm{G}} - \mathbf{u}_{\mathrm{L}}|$$

for the momentum exchange term where $(1/(U_{\mathrm{G}}/\varepsilon_{\mathrm{G}}^{\mathrm{B}})^2)$ $(1/\varepsilon_{\mathrm{L}}^{\mathrm{B}})$ is estimated a priori from the Bennett relation. When above expression for the gas–liquid momentum

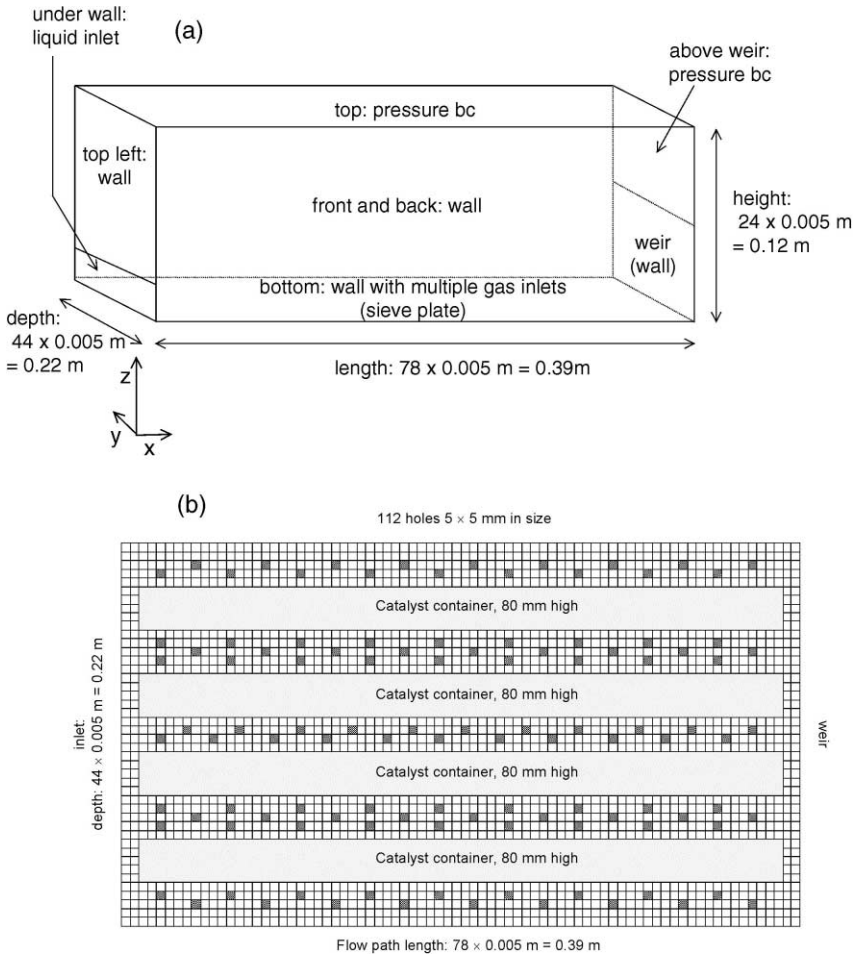

Fig. 2. (a) Computational space for CFD simulations. (b) Details of distributor plate used in the simulations.

exchange within the momentum balance relations the local, transient, values of $\mathbf{u}_G$, $\mathbf{u}_L$, ε_G and ε_L are used.

A commercial CFD package CFX 4.2 of AEA Technology, Harwell, UK, was used to solve the equations of continuity and momentum for the two-fluid mixture. This package is a finite volume solver using body-fitted grids. The dimensions of the computational space are $0.39\,\text{m} \times 0.12\,\text{m} \times 0.22\,\text{m}$ as shown in Fig. 2(a). Grid cells of 5 mm size are used in the *x*-, *y*- and *z*-directions. The choice of the grid size is based on our experience gained in the modelling of gas–liquid bubble columns operating in the churn-turbulent regime; the chosen grid size of 5 mm is smaller than the smallest grid used in our earlier studies [18–22], where grid convergence was satisfied. The total number of grid cells within the computational space is $78 \times 24 \times 44 = 82\,368$. Fig. 2(b) shows the layout of holes at the sieve plate in the bottom of the system. The fractional free-area in the computations is the same as that used in the experiments; however, square holes (112 in number) are used in the simulations rather than circular holes because a rectangular Cartesian coordinate system is used. The catalyst containers are modelled as solid, impervious, blocks 80 mm high, 25 mm thick and 370 mm long. The simulations have been performed on a Silicon Graphics Power Challenge with six R10000 processors running in parallel at 200 MHz. A representative dynamic

simulation took about 2 days to attain steady state. From the simulation results, average liquid hold-up as a function of height has been determined. Dispersion height has been defined by the height at which the average liquid hold-up drops below 10%. Clear liquid height has been determined by calculating the total amount of liquid in the system. Average liquid hold-up has been calculated by dividing clear liquid height by dispersion height. Further details of the computational algorithms used, boundary conditions, including an animation of a typical simulation are available on our web site: http://ct-cr4.chem.uva.nl/kattray.

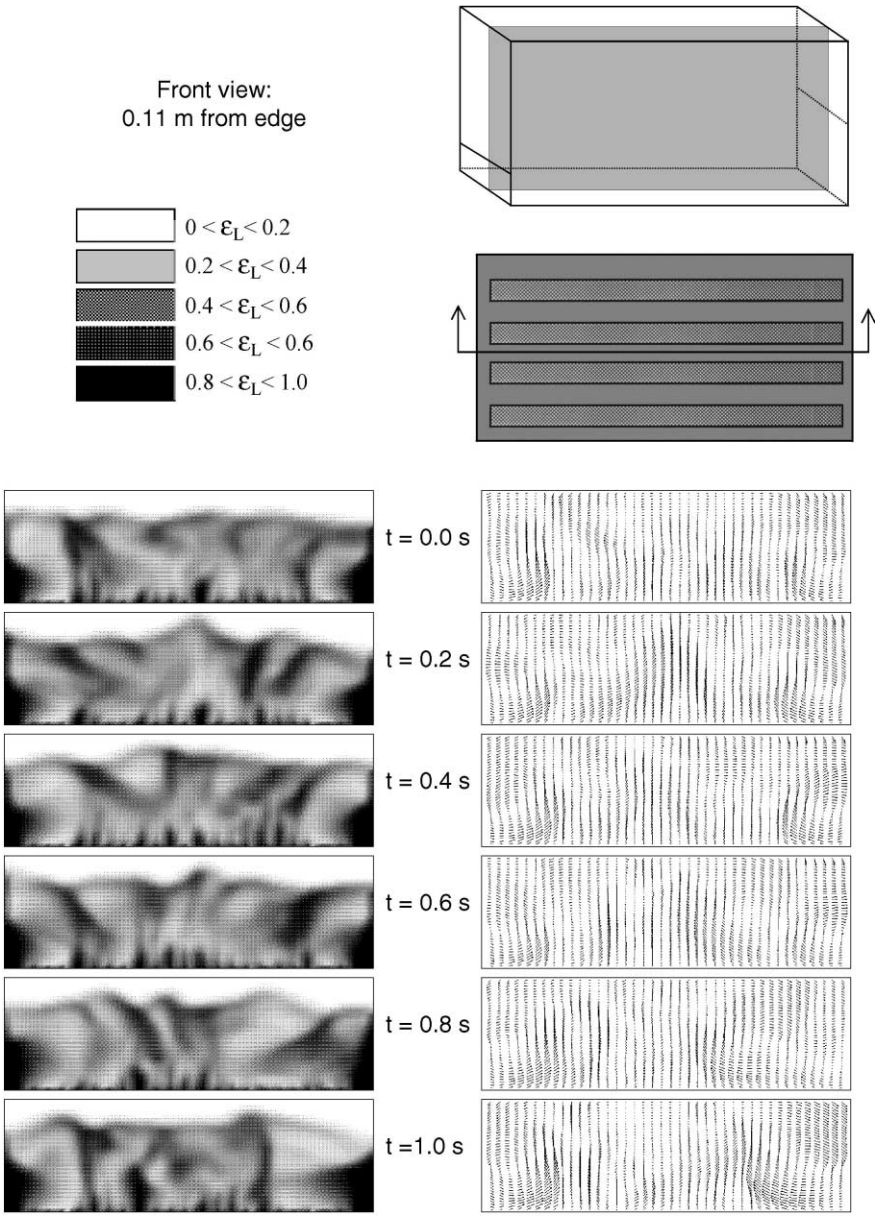

Fig. 3. Snapshots of liquid hold-up and liquid velocity vectors at different times. Animation on our web site: http://ct-cr4.chem.uva.nl/kattray.

Quasi-steady state values are obtained by running a dynamic simulation until no more changes in the total liquid hold-up in the system are observed. The largest time step used in the simulations is 2×10^{-3} s. Approach to quasi-steady state by monitoring the liquid in the system. Typically, 4000 time steps are required to attain quasi-steady state conditions. Steady state values of the clear liquid height, presented later in this work, have been taken from a time period in which the total amount of liquid in the system remained practically constant. Fig. 3 presents snapshots of the front view of the tray operating with catalyst containers. The slice is in between the two centre containers. Two liquid circulation zones, near the inlet and near the weir, can clearly be distinguished.

4. Experiments vs. CFD simulations

Fig. 4 presents typical simulation results for the variation of the liquid hold-up along the height of the dispersion. The values of the hold-up are obtained after volume-averaging along the *x*- and *y*-directions, ignoring the volume of the catalyst containers. The increase in liquid hold-up right above the weir height (equal to the catalyst container height) seen in this figure is caused by liquid sitting on top of the containers; this has also been observed experimentally. In the absence of containers (see Fig. 4(b)), there can be no such accumulation of liquid.

Fig. 5 compares the experimental data for the clear liquid height, h_{cl}, with the results from CFD simulations. For a constant liquid height and fixed weir height, the clear liquid height decreases with increasing superficial gas velocity U_G, see Fig. 5(a). The superficial gas velocity U_G is defined based on the area available for flow of gases (tray area minus the cross-sectional area occupied by the containers). When comparing the results with and without containers, we note that the presence of the containers tends to increase h_{cl}; this is due to the suppression of the large-scale liquid circulations. For a constant superficial gas velocity and liquid load, increasing the weir height tends to increase h_{cl}, see Fig. 5(b). For reactive distillation application, the liquid hold-up is an important parameter because it will determine the residence time of the liquid on the tray. Large weir heights are to be used to increase the liquid residence time. It is to be noted that for conventional distillation, weir heights are usually limited to below about 50 mm and the operation is in the spray regime. For reactive distillation, much higher weirs are to be used and the operation in the bubbly froth regime is preferred. With increasing liquid load per unit length of weir, Q_L/W, the clear liquid height increases, see Fig. 5(c). Considering the fact that the only empirical input to the CFD simulations is the Bennett relation in calculating $\mathbf{M}_{L,G}$, the agreement between CFD simulations and experiment is remarkably good.

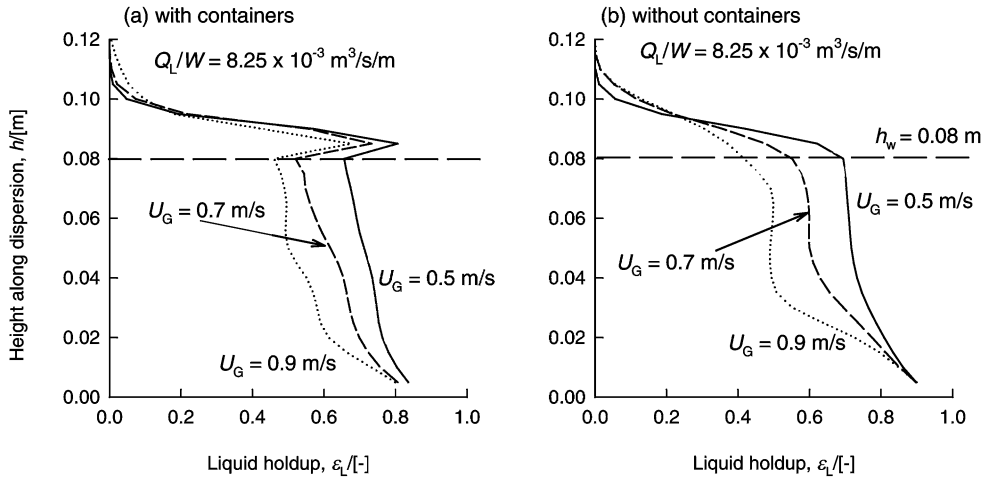

Fig. 4. Liquid hold-up profiles along the height of dispersion on tray from CFD simulations for (a) sieve tray without containers, and (b) sieve tray with catalyst containers.

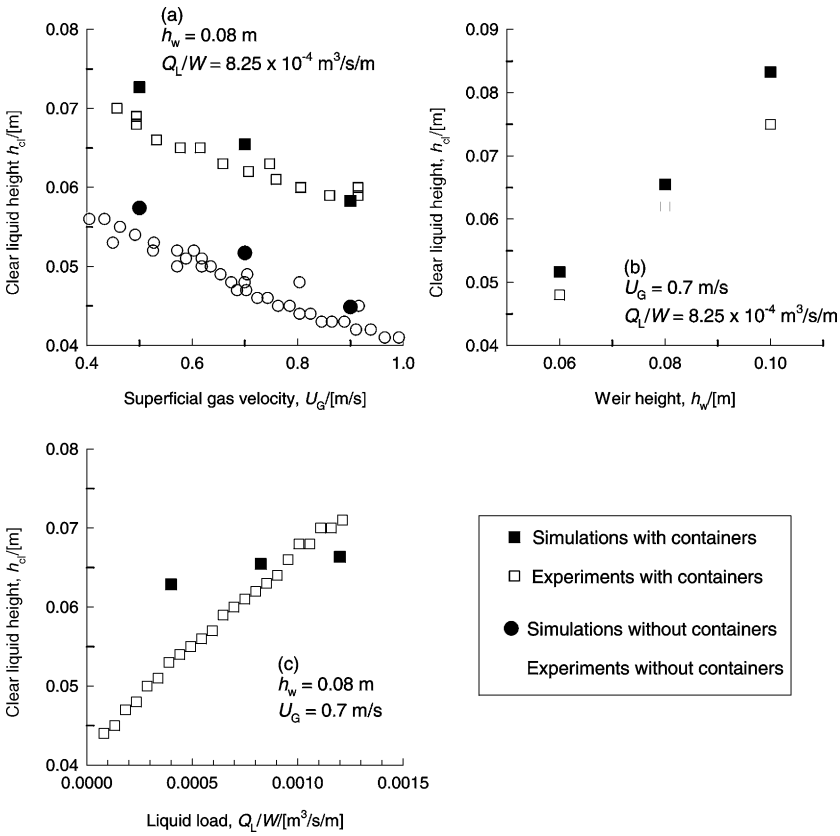

Fig. 5. Comparison of experiments vs. CFD simulations of clear liquid height.

5. Conclusions

In this, we have studied the hydrodynamics of a novel contactor for reactive distillation. Catalyst containing wire-gauze envelopes are disposed along the liquid flow path of a sieve tray column. The staging in the liquid flow direction is beneficial for RD applications. The experiments and CFD simulation work focussed on the most important parameter determining the sieve tray, namely the clear liquid height. The clear liquid height is an essential parameter in the estimation of tray hydrodynamics and mass transfer in sieve tray columns [24] and it is heartening to note that CFD techniques allow the estimation of this parameter for a catalytic distillation tray. Our CFD model is now considered to be validated.

The strategy we advocate is to use this validated CFD technique for design and scale up of catalytic distillation trays. With CFD simulations, we obtain detailed information of liquid velocity distributions, hold-up distributions, dispersion, etc. Such information is required for a rational design of catalytic distillation columns.

Acknowledgements

The Netherlands Organisation for Scientific Research (NWO) is gratefully acknowledged for providing financial assistance in the form of a “programmasubsidie”.

References

[1] R. Taylor, R. Krishna, Chem. Eng. Sci. 55 (2000) 5183.
[2] C. Van Gulijk, Comput. Chem. Eng. 22 (1998) S767.

[3] J. Ellenberger, R. Krishna, Chem. Eng. Sci. 54 (1999) 1339.
[4] A.P. Higler, R. Krishna, J. Ellenberger, R. Taylor, Chem. Eng. Sci. 54 (1999) 5145.
[5] R. Krishna, J.M. van Baten, J. Ellenberger, A.P. Higler, R. Taylor, Chem. Eng. Res. Des., Trans. Inst. Chem. Engrs. 77 (1999) 639.
[6] J.M. van Baten, R. Krishna, Chem. Eng. J. 77 (2000) 143.
[7] J.L. DeGarmo, V.N. Parulekar, V. Pinjala, Chem. Eng. Prog. 3 (1992) 43.
[8] A.P. Gelbein, M. Buchholz, US Patent 5 073 236 (1991).
[9] K.H. Johnson, A.B. Dallas, US Patent 5 348 710 (1994).
[10] P. Moritz, H. Hasse, Chem. Eng. Sci. 54 (1999) 1367.
[11] J.P. Stringaro, European Patent 43 322 2A1 (1991).
[12] J.P. Stringaro, US Patent 5 470 542 (1995).
[13] E.M. Jones Jr., US Patent 4 536 373 (1985).
[14] R. Krishna, J.M. van Baten, Nature 398 (1999) 208.
[15] R. Krishna, M.I. Urseanu, J.M. van Baten, J. Ellenberger, Int. Commun. Heat Mass Transfer 26 (1999) 781.
[16] R. Krishna, J.M. van Baten, Int. Commun. Heat Mass Transfer 26 (1999) 965.
[17] R. Krishna, J.M. van Baten, M.I. Urseanu, J. Ellenberger, Chem. Eng. Process. 39 (2000) 433.
[18] R. Krishna, M.I. Urseanu, J.M. van Baten, J. Ellenberger, Chem. Eng. Sci. 54 (1999) 171.
[19] R. Krishna, M.I. Urseanu, J.M. van Baten, J. Ellenberger, Chem. Eng. Sci. 54 (1999) 4903.
[20] R. Krishna, J.M. van Baten, M.I. Urseanu, Chem. Eng. Sci. 55 (2000) 3275.
[21] R. Krishna, M.I. Urseanu, J.M. van Baten, J. Ellenberger, Chem. Eng. J. 78 (2000) 43.
[22] R. Krishna, Oil Gas Sci. Technol. 55 (2000) 359.
[23] D.L. Bennett, R. Agrawal, P.J. Cook, AIChE J. 29 (1983) 434.
[24] M.J. Lockett, Distillation Tray Fundamentals, Cambridge University Press, Cambridge, 1986.